Chinese Chemical Letters 36 (2025) 109934

Contents lists available at ScienceDirect

Chinese Chemical Letters

journal homepage: www.elsevier.com/locate/cclet

# Fluorine-functionalized zirconium-organic cages for efficient photocatalytic oxidation of thioanisole

Jia-Ru Li[a,b], Ning Li[b,*], Li-Ling He[b], Jun He[a,*]

[a] School of Chemical Engineering and Light Industry, Guangdong University of Technology, Guangzhou 510006, China
[b] School of Chemistry, South China Normal University, Guangzhou 510006, China

ARTICLE INFO

*Article history:*
Received 13 March 2024
Revised 4 April 2024
Accepted 28 April 2024
Available online 6 November 2024

*Keywords:*
Ultraviolet light
Fluorine
Zirconium-based metal-organic cages
Sulfide oxidation
Multiphase photocatalysis

ABSTRACT

Zirconium-based metal-organic cages (Zr-MOCs) typically exhibit high stability, but their structural and application reports are scarce due to stringent crystallization conditions. We have successfully fluorinated the classical Zr-MOCs (**ZrT-3**) for the first time, obtaining the fluorinated MOCs (**ZrT-3-F**). Notably, **ZrT-3-F** not only inherits the high stability of its parent structure, but also acts as a catalyst for the effective oxidation of benzyl thioether for the first time. The reaction can reach a conversion rate of 99% in 6 h, and the selectivity reaches 95%, which far exceeds the non-fluorinated **ZrT-3**. This work proves that the specific functionalization of the classical Zr-MOCs can further expand their application potential, such as catalysis.



Metal-organic cages (MOCs) are individual supramolecular units created from metal nodes and organic connectors. Despite their assembly and structure being similar to metal-organic frameworks (MOFs), the MOCs, structured at the nanoscale level, exhibit unique attributes in terms of size, topology, solubility, characterization, and stability [1]. So far, a variety of MOCs have been documented, including those derived from rhodium (Rh), iron (Fe), cobalt (Co), titanium (Ti), and zirconium (Zr) [2-6]. The high bond energies of metal-oxygen bonds impart considerable structural stability to these MOCs. In particular, the Zr-O bond, with its energy of $766.1 \pm 10.6$ kJ/mol, results in Zr-MOCs exhibiting greater stability compared to MOCs based on other metals. Nevertheless, there have been few reported instances of Zr-MOCs, with research into their application performances also being greatly limited [7,8]. During the synthesis of Zr-MOCs, the susceptibility of Zr to oxidation poses a challenge. Zr being a reactive transition metal, readily reacts with oxygen to form oxides, especially under conditions of elevated temperature, humidity, or exposure to air. This tendency contributes to the scarcity of reported Zr-MOCs structures, thereby limiting their applications in performance.

To expand the performance research of Zr-MOCs, functionalizing modifications of the ligands of MOCs can be employed. Numerous studies have shown that incorporating functional groups into the organic ligands of MOCs can enhance their applications in various aspects [1,9-11]. Introducing Lewis basic functional groups (such as hydroxyl, amino, carboxyl, cyano, carbonyl, and fluorine) can enhance the selectivity and catalytic efficiency of specific organic reactions. Fluorine-functionalized MOCs exhibit characteristics such as fluorophilicity, electrostatic interactions, and anion-$\pi$ stacking. Moreover, due to the high electronegativity of fluorine, the C-F bond possesses high bond energy (110 kJ/mol), leading to the high chemical stability of C-F bonds [12-17]. Furthermore, the high electronegativity of fluorine results in greater electron density toward the fluorine side in covalent bonds. This induces a shift in the electron energy levels within the molecular orbitals (MOs), elevating energy levels for atoms connected to fluorine and lowering energy levels for fluorine atoms. This facilitates redox reactions, making MOCs more widely applicable. Among the reported Zr-MOCs, the most classic are **ZrT-1**, **2**, **3**, **4** reported by Yuan in 2013 [18]. Over the past decade, various research groups have conducted numerous functionalization modifications on the cages reported by Yuan [18]. For example, Su's group reported amino modifications on ligands, enabling their application in photocatalytic hydrogen evolution reactions [19]. However, their application in photocatalytic organic reactions is relatively limited.

Building upon the achievements of Yuan in 2013 [18], where the classical **ZrT-3** was employed, we fluorinated the organic ligands to synthesize $H_2$bpdc-8F as a fluorine-rich linker (Fig. 1). Using solvent-thermal synthesis, we then combined $H_2$bpdc-8F with Zirconocene dichloride ($Cp_2ZrCl_2$) to produce a tetrahedral-shaped Zr-MOCs: **ZrT-3-F**, with a molecular formula of $\{[Cp_3Zr_3\mu_3\text{-}O(\mu_2\text{-}OH)_3]_4(bpdc8F)_6\}\cdot 4Cl\cdot nS$ (where S = noncoordinated solvent molecule). It is noteworthy that the fluorinated cage exhibited

* Corresponding authors.
*E-mail addresses:* ningl0314@163.com (N. Li), junhe@gdut.edu.cn (J. He).

https://doi.org/10.1016/j.cclet.2024.109934
1001-8417/

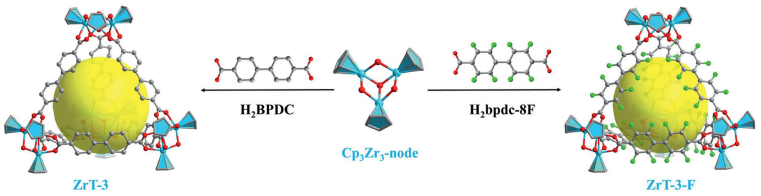


**Fig. 1.** Contrast sample: **ZrT-3** (left), **ZrT-3-F** (right), bridging ligands and trinuclear zirconium clusters.

higher stability and enhanced light absorption capabilities. Utilizing these advancements, we applied the fluorinated cage for the first time in the oxidation of benzyl sulfide to the sulfoxide reaction. In photocatalytic reaction experiments, we observed that the fluorinated cage demonstrated a selectivity and conversion rate of over 95% for sulfoxide, significantly surpassing the performance of the non-fluorinated cage.

The compound **ZrT-3-F** is produced *via* a solvent-thermal procedure, combining $Cp_2ZrCl_2$ and $H_2$bpdc-8F in a mixed solvent environment of dimethylacetamide (DMA), trichloromethane ($CHCl_3$), and $H_2O$. The exact synthesis route can be found in the supplementary materials provided. Utilizing X-ray single crystal diffraction analysis, we determined that **ZrT-3-F** crystallizes in the cubic *Fm*-3 *m* space group. The compound forms a distinctive $V_4E_6$ type cage, as previously documented by Yuan. The structure of **ZrT-3-F** consists of four secondary building units (SBUs), namely $Cp_3Zr_3\mu_3$-O($\mu_2$-OH)$_3$, and six $H_2$bpdc-8F linkers. The $Cp_3Zr_3\mu_3$-O($\mu_2$-OH)$_3$ unit acts as the vertex (V), while $H_2$bpdc-8F functions as the edges (E) of the tetrahedron. Due to the high symmetry of **ZrT-3-F**, the linking ligands exhibit significant disorder. The interspace between two SBUs measures 15.387 Å, resulting in an approximate internal volume of the cage of 139.2 Å$^3$, as derived from calculations.

To evaluate the high photocatalytic activity potential of **ZrT-3-F**, a thorough investigation into its optical and electronic properties was conducted. Additionally, a comparative analysis between **ZrT-3-F** and **ZrT-3** was carried out to elucidate key disparities in band structure and charge carrier behavior. UV/visible diffuse reflectance spectroscopy (DRS) measurements indicated that **ZrT-3-F** exhibited nearly full-spectrum absorbance, including visible light absorption between 400 nm and 480 nm, unlike **ZrT-3** which primarily absorbed in the UV region (Fig. 2a). Bandgap energies were computed using the Kubelka-Munk function equation: $\alpha h\nu = A(h\nu - E_g)^{1/2}$.

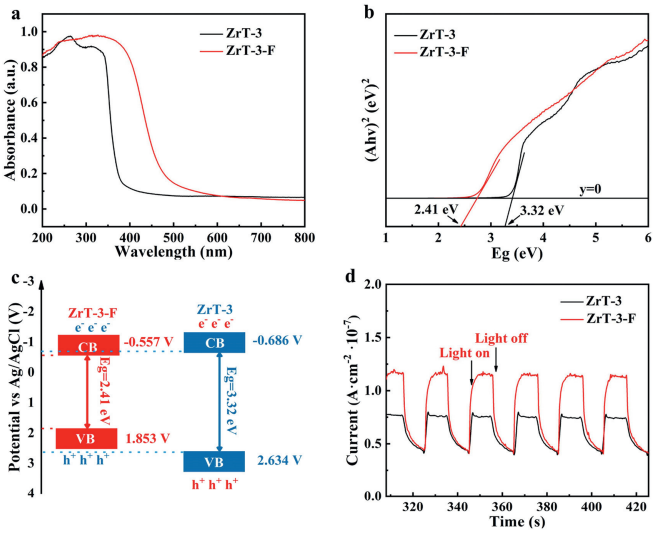


**Fig. 2.** (a) UV–vis DRS spectra of **ZrT-3-F** (red) and **ZrT-3** (black). (b) Band gaps of **ZrT-3-F** (red) and **ZrT-3** (black). (c) Electronic band structure. (d) Photocurrent responses of **ZrT-3-F** (red) and **ZrT-3** (black).

The direct bandgap energies of **ZrT-3-F** and **ZrT-3** were estimated to be 2.41 and 3.32 eV, respectively, based on transformed differential spectra (Fig. 2b). Electronic band structures were determined by estimating conduction band (CB) potentials *via* Mott-Schottky (M-S) plots at frequencies of 1000, 1500, and 2000 Hz in the dark. Both **ZrT-3-F** and **ZrT-3** M-S plots exhibited positive slopes across all frequencies, consistent with n-type semiconductor characteristics (Figs. S9 and S10 in Supporting information) [20]. Flat band potentials ($V_{FB}$) were extrapolated to be –0.757 and –0.886 V *vs.* Ag/AgCl for **ZrT-3-F** and **ZrT-3**, respectively. Consequently, the CB potentials for **ZrT-3-F** and **ZrT-3** were –0.557 and –0.686 V, respectively. Using the formula $E_{CB} = E_{VB} - E_g$ [21], VB positions for **ZrT-3-F** and **ZrT-3** were calculated as 1.853 and 2.634 V, respectively, corresponding to the band structure arrangement (Fig. 2c). Furthermore, photocurrent response tests revealed a substantial increase in current under light irradiation compared to dark conditions. Notably, the photocurrent of **ZrT-3-F** consistently exceeded that of **ZrT-3**, irrespective of light exposure (Fig. 2d).

The process of converting sulfides into sulfoxides *via* aerobic oxidation finds extensive usage in sectors such as fossil fuel desulfurization, medicinal synthesis, and wastewater management [22,23]. In conventional synthesis methods, the elevated oxidation potentials of sulfides may induce over-oxidation reactions, generating undesired by-products [24-26]. Consequently, an efficacious photocatalyst is required for the successful aerobic oxidation of sulfides to sulfoxides [27,28].

An investigation on the photocatalytic performance of **ZrT-3-F** was carried out, utilizing the aerobic oxidation of sulfides to sulfoxides reaction. To determine the type of reaction products, a gas chromatography-mass spectrometry (GC–MS) was employed and quantification was conducted using a 50-bit ALS gas chromatograph. Since the main light absorption of **ZrT-3-F** lies in the ultraviolet region, UV light was adopted as the light source for the catalytic reaction. Initially, the choice of the best solvent was required, using oxygen as the oxidant. The selected solvents: *N*,*N*-Dimethylformamide (DMF), methanol ($CH_3OH$), isopropanol (IPA), and acetonitrile ($CH_3CN$) were put under consideration. The conversion and selectivity of $CH_3OH$ and $CH_3CN$ are the highest with the catalyst being homogeneous and heterogeneous in $CH_3OH$ and $CH_3CN$ respectively. From the standpoint of recyclability, the heterogeneous catalyst is more appropriate and hence $CH_3CN$ was selected as the reaction solvent. Subsequently, it was necessary to elect the right oxidant: even though $O_2$, hydrogen peroxide ($H_2O_2$), and *tert*-butyl hydroperoxide (TBHP) all achieved conversion rates up to 99%, $O_2$ proved to be the most optimal oxidant regarding product selectivity. Upon conducting experiments with varying masses of the catalyst, the results indicate that the optimal catalyst loading is 10 mg.

The optimal experimental conditions are as follows: 0.1 mmol of substrate, 3 mL of $CH_3CN$, and 10 mg of catalyst are added into a 10-mL quartz tube. The photocatalytic reaction is then performed for 6 h under 1 atm of oxygen and ultraviolet light irradiation. When **ZrT-3-F** is used as the catalyst, the conversion rate reaches up to 99.51% and selectivity up to 95.16%. In contrast, when **ZrT-3** is used as the catalyst in the experiment, the conversion rate of benzyl sulfide is only 21.44%, and the selectivity is only 66.7%.

**Table 1**
Photocatalytic oxidation of thioanisole catalyzed by the **ZrT-3-F**.

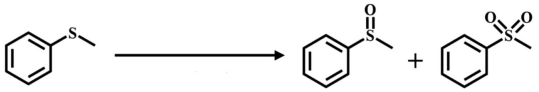

| Entry | Solvent | Light | Oxidizing agent | Photocatalyst | Mass of catalyst (mg) | Conversion (%) | Sulfoxide selectivity (%) | Sulfone selectivity (%) | Heterogeneous catalyst |
|---|---|---|---|---|---|---|---|---|---|
| 1[a] | $CH_3CN$ | + | $O_2$ | **ZrT-3-F** | 10 | 99.51 | 95.16 | 4.84 | + |
| 2[b] | $CH_3CN$ | + | TBHP | **ZrT-3-F** | 10 | 99.10 | 70.42 | 29.58 | + |
| 3[c] | $CH_3CN$ | + | $H_2O_2$ | **ZrT-3-F** | 10 | 99.50 | 60.41 | 39.59 | + |
| 4[a] | DMF | + | $O_2$ | **ZrT-3-F** | 10 | 99.60 | 80.23 | 19.77 | – |
| 5[a] | IPA | + | $O_2$ | **ZrT-3-F** | 10 | 99.30 | 72.68 | 27.32 | – |
| 6[a] | $CH_3OH$ | + | $O_2$ | **ZrT-3-F** | 10 | 99.20 | 95.20 | 4.80 | – |
| 7[d] | $CH_3CN$ | + | None | **ZrT-3-F** | 10 | 24.56 | 95.44 | 4.56 | + |
| 8[e] | $CH_3CN$ | + | $O_2$ | **ZrT-3-F** | 5 | 73.45 | 95.46 | 4.54 | + |
| 9[f] | $CH_3CN$ | + | $O_2$ | None | 0 | 0 | 0 | 0 | / |
| 10[a] | $CH_3CN$ | + | $O_2$ | $H_2$bpdc-8F | 10 | 52.67 | 96.67 | 3.33 | + |
| 11[a] | $CH_3CN$ | + | $O_2$ | $Cp_2ZrCl_2$ | 10 | 51.48 | 58.29 | 41.71 | + |
| 12[a] | $CH_3CN$ | + | $O_2$ | **ZrT-3** | 10 | 21.44 | 66.70 | 33.30 | + |
| 13[g] | $CH_3CN$ | – | $O_2$ | **ZrT-3-F** | 10 | 1.62 | 95.43 | 4.57 | + |

[a] Thioanisole (0.1 mmol), Cat. (10 mg), solvent (3.0 mL), 1 atm. $O_2$, room temperature, 6.0 h, UV-light, products were analyzed by GC–MS.
[b] Thioanisole (0.1 mmol), Cat. (10 mg), $CH_3CN$ (3.0 mL), TBHP (20 μL), room temperature, 6.0 h, UV-light, products were analyzed by GC–MS.
[c] Thioanisole (0.1 mmol), Cat. (10 mg), $CH_3CN$ (3.0 mL), $H_2O_2$ (20 μL, 30 wt%), room temperature, 6.0 h, UV-light, products were analyzed by GC–MS.
[d] Thioanisole (0.1 mmol), **ZrT-3-F** (10 mg), $CH_3CN$ (3.0 mL), room temperature, 6.0 h, UV-light, products were analyzed by GC–MS.
[e] Thioanisole (0.1 mmol), **ZrT-3-F** (5 mg), $CH_3CN$ (3.0 mL), 1 atm $O_2$ room temperature, 6.0 h, UV-light, products were analyzed by GC–MS.
[f] Thioanisole (0.1 mmol), $CH_3CN$ (3.0 mL), 1 atm $O_2$ room temperature, 6.0 h, UV-light, products were analyzed by GC–MS.
[g] Thioanisole (0.1 mmol), **ZrT-3-F** (10 mg), $CH_3CN$ (3.0 mL), 1 atm $O_2$ room temperature, 6.0 h, products were analyzed by GC–MS.

When the organic ligand $H_2$bpdc-8F is used, the conversion rate is 52.67%, and the selectivity is 96.67%. When $Cp_2ZrCl_2$ is used as the catalyst, the conversion rate is 51.48%, and the selectivity is 58.29%. In summary, in this experimental system, the catalyst **ZrT-3-F** has the highest value (Table 1).

Next, the wide-ranging suitability of **ZrT-3-F** as a heterogeneous photocatalyst was put under scrutiny, assessing the transformation rates and selectivity amongst various sulfides. As shown in the table, all the chosen sulfides demonstrated over 90% selectivity and conversion to sulfoxides. Table 2 shows a marked drop in the conversion performance when the para-position on the sulfur is electron-absorbing, confirming that electron-donating para-substituents are more conducive to the photocatalytic oxidation of thioanisole to its corresponding sulfoxide under aerobic conditions.

The photostability of **ZrT-3-F** was evaluated through several centrifugations processed and washed with $CH_3CN$. Upon conducting three repeated experiments with **ZrT-3-F** (Fig. 3a), it was found that the reactive capacity of the catalyst did not decrease significantly. The catalyst harvested after the cycle was put through Fourier transform infrared (FT-IR) spectroscopy (Fig. S16 in Supporting information), with the spectral results demonstrating negligible differences between the pre-reaction and post-reaction spectrums. This indicates that the structure remained unaffected. According to these findings, **ZrT-3-F** demonstrates exceptional stability as a heterogeneous photocatalyst.

To delve into the fundamental reaction mechanism responsible for the photocatalytic oxidation of thioanisole into sulfoxide under aerobic conditions, a sequence of radical quenching experiments was performed (Fig. 3b). Utilizing 2,6-di-*tert*-butyl-*p*-cresol (BHT)

**Table 2**
Photocatalytic selective oxidation of sulfides to sulfoxide over **ZrT-3-F**.

| Entry | Substrate | Product | Conversion (%) | Sulfoxide selectivity (%) | Sulfone selectivity (%) |
|---|---|---|---|---|---|
| 1[a] |  |  | 99.51 | 95.16 | 4.84 |
| 2[a] | 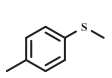 | 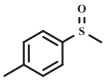 | 94.31 | 90.41 | 9.59 |
| 3[a] | 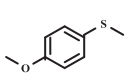 | 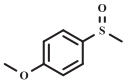 | 98.08 | 91.23 | 8.77 |
| 4[b] | 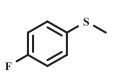 | 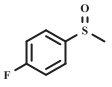 | 93.63 | 93.27 | 6.73 |
| 5[b] | 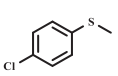 | 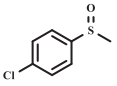 | 91.25 | 92.33 | 7.63 |
| 6[b] | 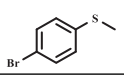 | 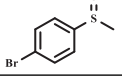 | 95.93 | 93.90 | 6.10 |

[a] Substrate (0.1 mmol), **ZrT-3-F** (10 mg), $CH_3CN$ (3.0 mL), $O_2$, room temperature, 6.0 h, products were analyzed by GC–MS.
[b] Substrate (0.1 mmol), **ZrT-3-F** (10 mg), $CH_3CN$ (3.0 mL), $O_2$, room temperature, 12 h, products were analyzed by GC–MS.

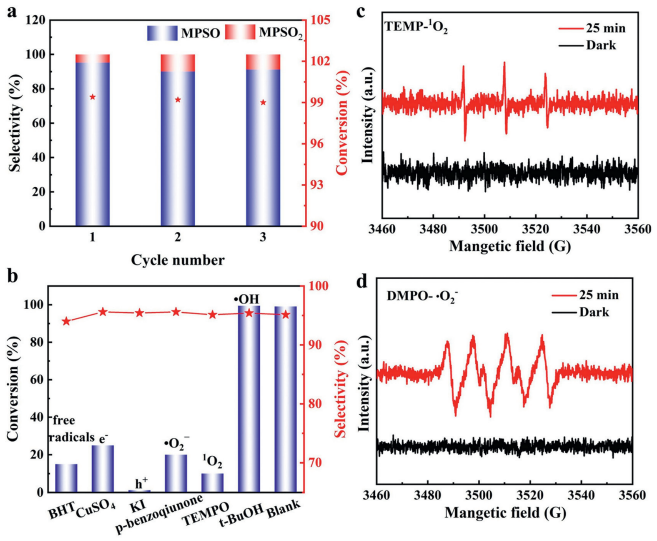


**Fig. 3.** (a) Stability of the **ZrT-3-F** photocatalyst for the selective aerobic oxidation of thioanisole under ultraviolet light. (b) Effect of scavengers on the photocatalytic oxidation of thioanisole. Reaction conditions: thioanisole (0.1 mmol), **ZrT-3-F** (10 mg), $CH_3CN$ (3.0 mL), $O_2$ (1 atm), 300 W Xe lamp ($\lambda = 200–400$ nm), room temperature, 6.0 h. EPR detection of *in situ* formed (c) $^1O_2$ using TEMP as a spin-trapping agent and (d) $^{\bullet}O_2^-$ radical using DMPO as radical trapping agent.

as a radical quenching agent, the production of reaction outputs was inhibited to a significant extent. This finding denotes the involvement of free radicals in this reaction. The subsequent introduction of copper sulfate ($CuSO_4$), acting as an electron inhibitor, caused a noticeable reduction in catalytic conversion efficiency. The implementation of potassium iodide (KI) as a hole inhibitor induced a state wherein the substrate underwent nearly no conversion, attesting to the occurrence of a photo-induced electron-hole ($e^-$-$h^+$) separation process in the reaction [29,30]. To detect the presence of reactive oxygen species (ROS) generated during the reaction, *tert*-butyl alcohol was added to quench any potential hydroxyl radicals ($^{\bullet}OH$). The lack of any conspicuous effect on conversion rates post its addition provided the evidence that $^{\bullet}OH$ radicals are not produced within this reaction framework. When *p*-benzoquinone and 2,2,6,6-tetramethylpiperidin-1-oxyl (TEMPO) were incorporated for trapping superoxide anion radical ($^{\bullet}O_2^-$) and singlet oxygen ($^1O_2$) respectively, a sharp decline in conversion rates was observed. This observation conclusively established that the ROS involved in this reaction are $^{\bullet}O_2^-$ and $^1O_2$ [30,31].

To further validate the existence of ROS in the reaction, electron paramagnetic resonance (EPR) experiments were implemented. The spin trap agent selected for the $^{\bullet}O_2^-$ was 5,5-dimethyl-1-pyrroline *N*-oxide (DMPO), while 2,2,6,6-tetramethylpiperidine (TEMP) was utilized for trapping singlet oxygen $^1O_2$. As depicted in the accompanying Figs. 3c and d, both $^{\bullet}O_2^-$ and $^1O_2$ demonstrated a significant response under photonic exposure, while no noticeable response was registered in dark conditions.

In conclusion, the conceivable mechanism for the photolytic conversion of phenyl methyl sulfide to sulfoxide (Fig. 4) involves UV light irradiation on **ZrT-3-F**, instigating the production of photo-generated electrons and holes. These photo-generated electrons swiftly disperse towards the surface of the catalyst and into the conduits where $O_2$ is reduced by the photoelectrons, resulting in $^{\bullet}O_2^-$. Neutral exciton-forming entities possessing robust Coulomb interactions undergo a transition from the singlet excited state ($S_1$) to the low-energy triplet state ($T_1$) *via* inter-system crossing (ISC) [32]. In this scenario, the energy is ceded to the attached $O_2$ molecules, leading to the production of $^1O_2$ and phosphorescence. Upon acquisition of a proton, the sulfide transforms

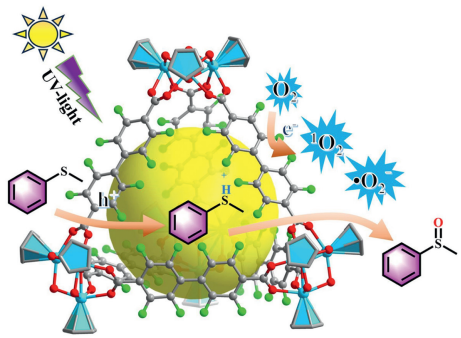


**Fig. 4.** Possible photocatalytic mechanisms.

into the free radical cation $CH_3SC_6H_5H^+$. $^{\bullet}O_2^-$ and $CH_3SC_6H_5H^+$ then initiate a nucleophilic reaction [33,34]. Concurrently, $^1O_2$ instigates an electrophilic reaction with the sulfide to create a sulfur peroxide intermediate. The reaction of the sulfide with the sulfur peroxide intermediate paves the way for the synthesis of sulfoxides. Notably, the end product of both mechanisms is sulfoxide [35].

Fluorination of the classical Zr-MOCs, such as **ZrT-3**, results in enhanced light absorption compared to the non-fluorinated cages. The fluorinated **ZrT-3** exhibits a stronger photocurrent response, thereby presenting advantages in photocatalytic reactions. Therefore, we employed **ZrT-3-F** for the oxidation of benzyl sulfide to sulfoxide. In photocatalytic reactions, **ZrT-3-F** serves as a heterogeneous catalyst under aerobic conditions, and achieves conversion rates and selectivity in oxidizing benzyl sulfide to sulfoxide. The conversion rate and selectivity are significantly higher compared to the performance of **ZrT-3** in catalytic reactions, demonstrating the excellent versatility and chemical stability of the catalyst throughout the reaction process. Importantly, this work demonstrates the applicability of fluorinated Zr-MOCs in organic catalysis.

## Declaration of competing interest

The authors declare that they have no known competing financial interests or personal relationships that could have appeared to influence the work reported in this paper.

## CRediT authorship contribution statement

**Jia-Ru Li:** Data curation, Investigation, Methodology, Writing – original draft, Writing – review & editing. **Ning Li:** Funding acquisition, Supervision, Writing – review & editing. **Li-Ling He:** Formal analysis, Validation. **Jun He:** Funding acquisition, Resources, Supervision.

## Acknowledgments

This work is supported by National Natural Science Foundation of China (Nos. 22201046, 22371054), Local Innovation Research Team Project of Guangdong Pearl River Talent Plan (No. 2017BT01Z032).

## Supplementary materials

Supplementary material associated with this article can be found, in the online version, at doi:10.1016/j.cclet.2024.109934.

## References

[1] E.M. El-Sayed, Y.D. Yuan, D. Zhao, et al., Acc. Chem. Res. 55 (2022) 1546–1560.
[2] S. Furukawa, N. Horike, M. Kondo, et al., Inorg. Chem. 55 (2016) 10843–10846.

[3] I. Papadaki, C.D. Malliakas, T. Bakas, et al., Inorg. Chem. 48 (2009) 9968–9970.
[4] S.T. Wang, X.H. Gao, X.X. Hang, et al., J. Am. Chem. Soc. 138 (2016) 16236–16239.
[5] Y.P. He, L.B. Yuan, G.H. Chen, et al., J. Am. Chem. Soc. 139 (2017) 16845–16851.
[6] Z.F. Ju, G.L. Liu, Y.S. Chen, et al., Chem. Eur. J. 23 (2017) 4774–4777.
[7] M.G. Sullivan, H.K. Welgama, M.R. Crawley, et al., Chem. Mat. 36 (2024) 567–574.
[8] B.X. Jiang, H. Wang, Y.T. Zhang, et al., Polyhedron 243 (2023) 116569.
[9] H.Y. Lin, Z.F. Xiao, K.N. Le, et al., Angew. Chem. Int. Ed. 61 (2022) e202214055.
[10] J.J. Jiao, C.X. Tan, Z.J. Li, et al., J. Am. Chem. Soc. 140 (2018) 2251–2259.
[11] W.H. Xing, H.Y. Li, X.Y. Dong, et al., J. Mater. Chem. A 6 (2018) 7724–7730.
[12] S. Lee, H. Jeong, D. Nam, et al., Chem. Soc. Rev. 50 (2021) 528–555.
[13] Q. Tian, S. Chen, M. Shi, et al., Sens. Actuator. B: Chem. 404 (2024) 135309.
[14] H.T. Chen, T. Zhang, S.R. Liu, et al., Inorg. Chem. 61 (2022) 11949–11958.
[15] Z.A. Qiao, S.S. Brown, J. Adcock, et al., Angew. Chem. Int. Ed. 51 (2012) 2888–2893.
[16] D.K. Dogutan, R. McGuire, D.G. Nocera, J. Am. Chem. Soc. 133 (2011) 9178–9180.
[17] S.S. Wang, L. Wang, M. Dakovic, et al., ACS Catal. 2 (2012) 230–237.
[18] G.L. Liu, Z.F. Ju, D.Q. Yuan, et al., Inorg. Chem. 52 (2013) 13815–13817.
[19] M. Sun, Q.Q. Wang, C. Qin, et al., Chem. Eur. J. 25 (2019) 2824–2830.
[20] H.F. Ye, R. Shi, X. Yang, Y. Chen, et al., Appl. Catal. B: Environ. 233 (2018) 70–79.
[21] X. Li, Y. Qi, G.Z. Yue, et al., Green Chem. 21 (2019) 649–657.
[22] Y.M. Li, M. Wang, X.F. Jiang, ACS Catal. 7 (2017) 7587–7592.
[23] A.K. Clarke, A. Parkin, R.J.K. Taylor, et al., ACS Catal. 10 (2020) 5814–5820.
[24] Q. Li, X.W. Lan, G.Y. An, et al., ACS Catal. 10 (2020) 6664–6675.
[25] X.Y. Wang, M.H. Liu, Y.X. Liu, et al., J. Am. Chem. Soc. 145 (2023) 26900–26907.
[26] X. Liang, Z.F. Guo, H.X. Wei, et al., Chem. Commun. 54 (2018) 13002–13005.
[27] M. Forchetta, F. Sabuzi, L. Stella, et al., J. Org. Chem. 87 (2022) 14016–14025.
[28] X.N. Zou, D.S. Zhang, T.X. Luan, et al., ACS Appl. Mater. Interfaces 13 (2021) 20137–20144.
[29] H.X. Wei, Z.F. Guo, X. Liang, et al., ACS Appl. Mater. Interfaces 11 (2019) 3016–3023.
[30] C.L. Su, R. Tandiana, B.B. Tian, J. Su, K.P. Loh, et al., ACS Catal. 6 (2016) 3594–3599.
[31] X.Y. Gu, X. Li, Y.H. Chai, et al., Green Chem 15 (2013) 357–361.
[32] Q.Q. Li, P.H. Pan, H. Liu, et al., Inorg. Chem. 62 (2023) 17182–17190.
[33] J. Jiang, R.C. Luo, X.T. Zhou, et al., Adv. Synth. Catal. 360 (2018) 4402–4411.
[34] H.D. She, H. Zhou, L.S. Li, et al., ACS Sustain. Chem. Eng. 6 (2018) 11939–11948.
[35] Q.S. Zhu, H.Y. An, T.Q. Xu, et al., Appl. Catal. A: Gen. 662 (2023) 119283.